Langmuir

Article

pubs.acs.org/Langmuir

Overgrowth of Gold Nanorods by Using a Binary Surfactant Mixture

Boris N. Khlebtsov,[†,‡,*] Vitaly A. Khanadeev,[†] Jian Ye,[§] Gleb B. Sukhorukov,[∥] and Nikolai G. Khlebtsov[†,‡]

[†]Institute of Biochemistry and Physiology of Plants and Microorganisms, Russian Academy of Sciences, 13 Prospekt Entuziastov, Saratov 410049, Russia

[‡]Saratov State University, 83 Ulitsa Astrakhanskaya, Saratov 410026, Russia

[§]Shanghai Engineering Research Center of Medical Device and Technology at Med-X, School of Biomedical Engineering, Shanghai Jiao Tong University, 1954 Huashan Road, Shanghai 200030, China

[∥]School of Engineering and Materials Science, Queen Mary, University of London, Mile End Road, London, E1 4NS, U.K.

Supporting Information

ABSTRACT: Seed-mediated surfactant-assisted growth is widely used as the most effective method for gold nanorod (NR) synthesis. Using prepared nanorods as seeds for further overgrowth can increase the dimensional tunability of the final particles. However, overgrowth in usual cetyltrimethylammonium bromide (CTAB) surfactant solutions leads to poor control of the final particle shape and size. In this work, we report an improved strategy to demonstrate the controllable overgrowth of gold NRs in the binary surfactant mixture sodium oleate (NaOL) + CTAB. This approach overcomes the difficulty of growing NR suspensions with small amounts of impurities. By controlling the total amount of added NR seeds, it is possible to tune the average length, diameter, and plasmon resonances of overgrown particles in a wide range. Together with the original NaOL + CTAB method developed by Murray and co-workers (*Nano Lett.* **2013**, *13*, 555), this overgrowth approach expands the dimensional and plasmonic tunability of the fabrication technology without any decrease in the monodispersity and purity of samples.

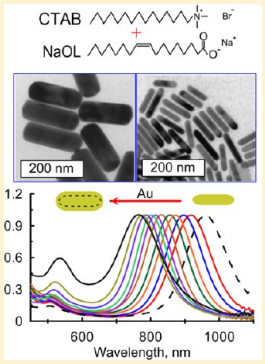

INTRODUCTION

Gold nanorods (NRs) have attracted substantial attention in recent years because of their unique optical properties and promising applications.[1] The shape anisotropy and rotational symmetry of small NRs lead to the appearance of two localized plasmon resonances (LPRs) in the extinction spectrum, corresponding to the transverse and longitudinal first-order plasmon modes.[2] For larger NRs with thicknesses of more than 20 nm and aspect ratios of more than 5, high-order plasmon modes can also be observed.[3−7] Typically, the transverse plasmon resonance is located at 505−520 nm, whereas the spectral position of the longitudinal LPR depends strongly on the NR aspect ratio and, therefore, can be synthetically tuned across a broad spectral range from 600 nm to the near-infrared (NIR) region. Furthermore, the scattering and absorption cross sections are determined by the total size of NRs.[8,9] For particles with equivolume diameters smaller than 30 nm, absorption makes the main contribution to the total extinction, whereas for larger NRs, scattering dominates. The unique optical properties make NRs an attractive platform for various applications,[1,10] including bioimaging,[11] surface-enhanced Raman scattering (SERS),[12−14] optical coherence tomography,[15,16] photothermal treatment of cancer cells and tumors,[17,18] chemical and biological sensing,[19−21] optoelectronic devices,[22] and so forth.

Since the seminal reports by the Wang,[23] Murphy,[24,25] and El-Sayed[26] groups, the seeded growth of particles in a CTAB solution has become the most popular method for NR synthesis. By varying the reagent concentration, one can adjust the NR length from tens to hundreds of nanometers, thus tuning the longitudinal resonance in a wide spectral range. However, the possibility of tuning the NR width through seed-mediated CTAB-assisted synthesis[27] is quite limited. More importantly, as-prepared (without additional purification[28−33]) NR suspensions usually contain a large amount of impurities.[28,30,34] Overgrowth and metal coating of NRs is a potential method for shape improvement and fine-tuning of LPRs. A few strategies for the secondary overgrowth of NRs have been reported in the literature and require the addition of gold ions and further chemicals[35−39] or stepwise addition of a reductant.[12,40] Despite these attempts, the formation of monodisperse thick gold NRs with a broadly tunable longitudinal resonance by the overgrowth technique has remained a challenge, especially with the use of surfactant (CTAB) alone and ascorbic acid as a reductant. Very recently, Murray's group[41,42] reported a novel method for NR synthesis by using a mixture of the CTAB and sodium oleate (NaOL) surfactants, which greatly improves the dimensional tunability of NR fabrication with controlled size, shapes, monodispersity, and purity.

In this paper, we show that the binary NaOL + CTAB mixture can be used not only for improved NR synthesis[41] but also for flexible overgrowth of NRs. This improvement overcomes the typical difficulties of CTAB-containing systems in overgrowing NRs while retaining their accurate cigarlike

Received: November 14, 2013
Revised: January 24, 2014
Published: January 27, 2014

   dx.doi.org/10.1021/la404399n | *Langmuir* 2014, 30, 1696−1703

shape and small amount of impurities. The main advantage of the overgrowth protocol is the accurate and convenient tuning of the dimensions and LPR wavelength of overgrown NRs by simple control over the molar ratio between seeded NRs and growth solution. Actually, one can achieve fine-tuning of the major LPR peak position with an accuracy of about 1 nm by simple monitoring of the reaction time.

EXPERIMENTAL SECTION

Materials. All chemicals were obtained from commercial suppliers and used without further purification. Cetyltrimethylammonium bromide (CTAB, >98.0%), sodium oleate (NaOL, technical grade; >82% fatty acid), L-ascorbic acid (>99.9%), hydrochloric acid (HCl, 37 wt % in water), and sodium borohydride ($NaBH_4$, 99%) were purchased from Sigma-Aldrich. Hydrogen tetrachloroaurate trihydrate ($HAuCl_4 \cdot 3H_2O$) and silver nitrate ($AgNO_3$, >99%) were purchased from Alfa Aesar. Ultrapure water obtained from a Milli-Q Integral 5 system was used in all experiments.

Fabrication of Original NRs. A 2−3 nm "seed" solution was prepared by adding 0.025 mL of 10 mM $HAuCl_4$ in 1 mL of aqueous 0.1 M CTAB. This was followed by adding 1 mL of 10 mM $NaBH_4$. The solution color changed from yellow to brownish yellow immediately after the addition of $NaBH_4$. The seed solution was aged at room temperature for 30 min before use in the next step.

For preparing the growth solution, 7.0 g of CTAB and 1.234 g of NaOL were dissolved in 250 mL of warm water (~50 °C). The solution was allowed to cool to 30 °C, and 18 mL of 4 mM $AgNO_3$ was added. The mixture was kept undisturbed at 30 °C for 15 min, after which 250 mL of 1 mM $HAuCl_4$ was added. The solution became colorless after 90 min of stirring, indicating the reduction of Au^{3+} to Au^{+}. The pH of the growth solution was adjusted by adding 2.1 mL of HCl (37 wt %). After another 15 min, 1.25 mL of 64 mM ascorbic acid and 0.8 mL of the seed solution were added. The resultant mixture was left undisturbed at 30 °C for 48 h for NR growth. During this time, the solution color varies continuously at a slow rate. In particular, the colorless solution became yellowish brown after 1 h, changed to brown after 2 h and then to dark brown (5 h), and finally changed to dark orange-brown (12−48 h). The absence of red and purple color during NR growth indicated a very low concentration of impurities.

Overgrowth of Gold Nanorods. To simplify our experimental procedure and to keep the CTAB + NaOL concentration unchanged, we used the same growth solution as described above for the overgrowth process. Twenty milliliters of the growth solution was mixed with an appropriate amount (1 to 20 mL) of as-prepared NRs to stimulate additional reduction of Au on the NR surface. No washings of the original NRs were conducted before overgrowth. The resultant mixtures were left undisturbed at 30 °C for 48 h for NR overgrowth. During the overgrowth period, the color of the solutions changed to reddish-brown, red, and pink, depending on the gold molar ratio between the growth solution and the original NRs.

Measurements. Transmission electron microscopy (TEM) images of the nanoparticles were obtained with a Libra-120 transmission electron microscope (Carl Zeiss, Germany) operating at 120 kV. NRs were deposited on a 300-mesh copper grid coated with Formvar. Extinction spectra were recorded with a Specord BS-250 UV−vis spectrophotometer (Analytik Jena, Germany) with a 2-mm optical path. Gold NR diameters and lengths were evaluated from digitized TEM images (Grapher 8, Golden Software, Inc.) of about 300 NRs.

Simulations. T-matrix simulations of NR extinction spectra with ensemble and orientation averaging were made as described in detail elsewhere.[43]

RESULTS AND DISCUSSION

Characterization of the Original NRs. Original NR suspensions were prepared by using the binary surfactant mixture (CTAB + NaOL) reported previously.[41] Figure 1a shows a TEM image of the original NRs with an aspect ratio of about 5, which is consistent with the results by Ye et al.[41]

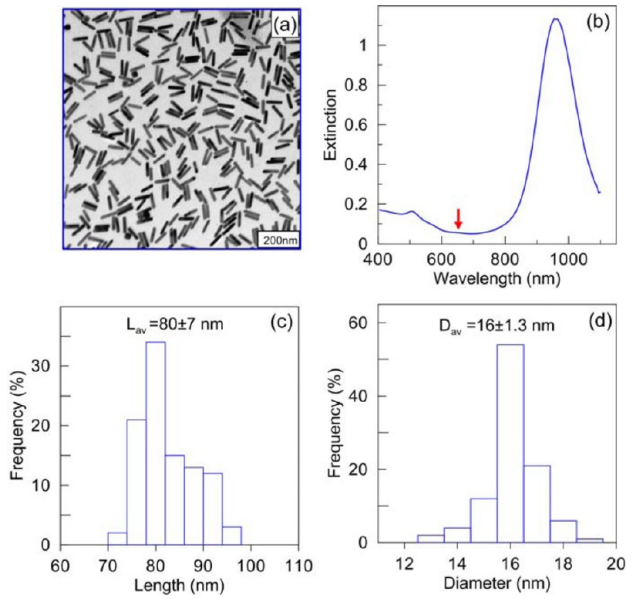

Figure 1. TEM image (a) and experimental extinction spectrum (b) of an as-prepared original NR suspension with a plasmon resonance at about 950 nm. Panels c and d show the NR length and width (diameter) histograms, respectively; the average length L_{av} and diameter D_{av} are indicated in the plots. The red arrow in panel b points to the minor quadrupole resonance.

Statistical analysis (Figure 1c and 1d) reveals that the NRs have a "cigarlike" shape with the average length 80 ± 7 nm and width 16 ± 1.3 nm. Note that TEM analysis reveals a very small percentage (less than 2%) of impurity particles in the sample. This fact can be attributed to the low concentration of CTAB used in the synthesis (0.037 M, by contrast to 0.1 M used in the common seed-mediated method[26]). An additional reason can be the slow reaction speed. Figure 1b shows a typical extinction spectrum of NRs with two well-known LPR peaks. For as-prepared original NRs, the longitudinal and transversal LPR modes are located near 950 and 507 nm, respectively. These resonances are typical of gold NRs with diameters of 15 nm and an aspect ratio of about 5. It has been shown previously[44] that a high ratio between the longitudinal and transverse resonance maxima, $A_2/A_1 = A_{\parallel}/A_{\perp}$, together with a weak extinction in the range 525−600 nm is indicative of the high quality of NR samples, with a small percentage of impurity particles. In our case, the ratio $A_{\parallel}/A_{\perp}$ has a remarkable value of about 7. In addition, there are no pronounced maxima or shoulders within the 525−600-nm spectral band, except for a minor maximum located near 650 nm (indicated by the red arrow in Figure 1b). This minor maximum can be attributed to quadrupole excitation,[3−5] which gives additional evidence that the synthesized NRs are of high quality.[4] On the other hand, the full width at half-maximum (fwhm) of the major longitudinal peak is about 150 nm, which is typical of the moderate polydispersity of NRs over length and width[45,46] shown in Figure 1c and 1d.

Overgrowth of Gold NRs. As the binary surfactant mixture produces "cigarlike" NRs, we assumed that overgrowth should work best under the same reaction conditions. By following this strategy, all experiments were performed by simply mixing the original NRs with the growth solution with a gold molar ratio R = growth solution/NRs from 1 to 20, followed by keeping the mixture at 30 °C for 24 h. After the overgrowth ended, NRs

dx.doi.org/10.1021/la404399n | Langmuir 2014, 30, 1696−1703

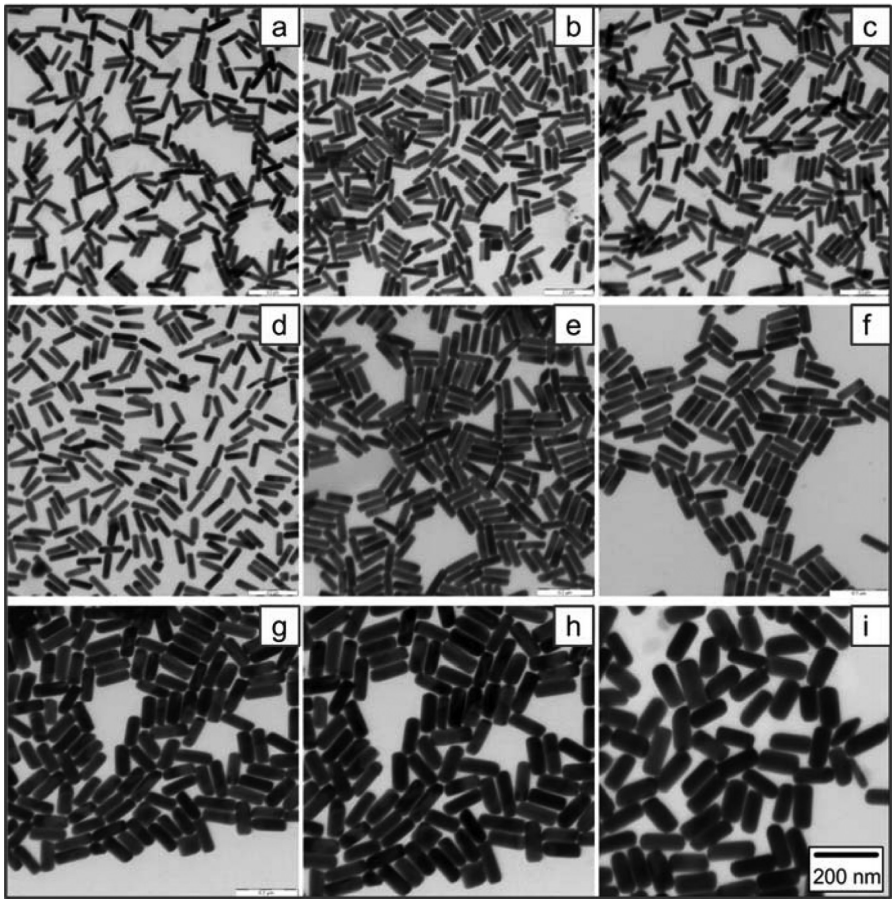

Figure 2. TEM images of NRs obtained by overgrowth at gold molar ratios of 2.22 (a), 2.5 (b), 2.85 (c), 3.33 (d), 4 (e), 5 (f), 6.66 (g), 10 (h), and 20 (i). Scale bars correspond to 200 nm for all images. No image adjustments were made.

were washed by centrifugation/redispersion in water at the same particle concentration, and the samples were studied by TEM and UV−vis spectroscopy.

Figure 2 shows TEM images collected for NR samples after overgrowth at molar ratios of the growth solution/original NRs ranging from 2.22 (Figure 2a) to 20 (Figure 2i). Note that all images are shown with the same magnification, scale bar, and contrast. Evidently, the overgrowth process led to an increase in both NR length and width, while the particles retained their original "cigarlike" morphology. Recently, several groups have reported crystallographic interpretations of the crystal facets for cigarlike NRs.[47,48] Following those reports and our preliminary high-resolution TEM data (see Figure S1 in Supporting Information), we believe that the overgrown NRs have a faceted shape and are enclosed {110} lateral facets. The ends of the NRs are enclosed by predominantly {111} and {100} planes.[36,41] Some minor shape transformations were observed at high molar ratios (Figure 2i) and became evident at very high ratios (from 40 to 200).

TEM and SEM images of cigarlike overgrown NRs are shown in Figure S2 (Supporting Information). Again, these images do not reveal any significant difference in the polydispersity index of NRs before and after overgrowth. It should be emphasized that the percentage of impurity particles (cubes, platelets, quasispheres, etc.) remains negligible in all samples. Statistical analysis (up to 300 particles) was made to systematize the results of the TEM experiment and to evaluate the average NR length, width, and aspect ratio.

To characterize the dimensional tuning of NRs by the overgrowth process, we used the length and width increments defined as the difference between the original and overgrown sizes: $\Delta L = L - L_0$ and $\Delta D = D - D_0$. Figure 3a shows the

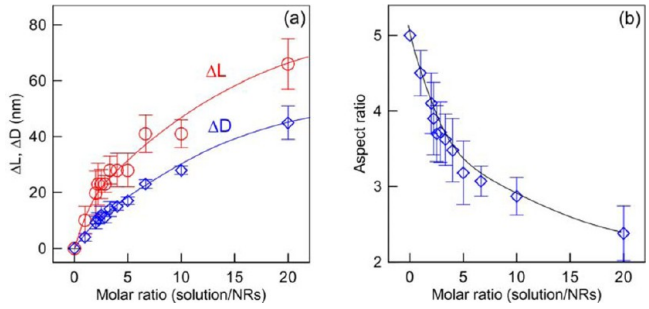

Figure 3. (a) Dependence of length (ΔL) and width (ΔD) increments on the gold molar ratio growth solution/seed NRs used in the overgrowth experiment. (b) The NR aspect ratio as a function of the molar ratio growth solution/seed NRs. Data were taken from a statistical analysis of the TEM images.

dependences of the average length and width increments on the gold molar ratio growth solution/seed NRs. The error bars show standard deviations calculated for each statistical ensemble of 300 NRs at a given molar ratio. The overgrowth process is clearly anisotropic, and at first glance, the NR elongation seems more effective than NR growth in the transversal direction at the same molar ratio. However, it

dx.doi.org/10.1021/la404399n | Langmuir 2014, 30, 1696−1703

follows from Figure 3b that the average ratio between the overgrowth rates along and perpendicularly to the NR axis is lower than the aspect ratio of the original NRs. This explains why the NR aspect ratio decreases from 5 (original NRs) to 2.4 (molar ratio of 20) during the overgrowth process.

The anisotropic nature of the process indicates that there is preferential overgrowth along the longitudinal axis rather than uniform deposition of an additional metal layer on the NR surface. The latter one is typical for reduction of silver[49] and other metal layers[50] on the surface of gold NRs. It has been shown that the longitudinal resonance of thick NRs is red-shifted as compared to thin NRs with the same aspect ratio.[51,52] However, as the NR aspect ratio is the main parameter determining the longitudinal resonance wavelength, we expect the overall blue-shift of the resonance during overgrowth.

Figure 4a shows normalized extinction spectra of NR samples taken before and after overgrowth at different gold molar ratios (molar ratio of 0 corresponds to the original NRs). During overgrowth, the longitudinal surface plasmon band gradually blue-shifted, while the transverse mode slightly red-shifted and intensified as well, finally becoming comparable in intensity with the longitudinal mode. In general, all spectra can be conventionally separated into three groups. During overgrowth at small gold molar ratios (from 0 to 2), the longitudinal resonance gradually shifts from 950 to 850 nm, while the transverse band remains almost constant. These changes can be attributed to increases in the NR length (from 80 to 100 nm) and width (from 16 to 25 nm). As a result, the aspect ratio decreases from 5 to 4 (see the red mark in Figure 4a and the red part of the NR parameters in Table S1, Supporting Information). After that, when the molar ratio increases from 2 to 5, the aspect ratio decreases more slowly from 3.9 to 3.53. Such a small decrement, together with the increase in both NR length and width, leads to an almost fixed location of the main plasmon mode near 850−840 nm. This regime corresponds to the green part in Table S1 (Supporting Information) and to the green mark in Figure 4a. Finally, the longitudinal plasmon resonance shifts from 850 to 750 nm when the molar ratio increases from 5 to 20. According to the TEM data, this stage is accompanied by an almost 2-fold increase in NR width (from 33 to 61 nm), which gives rise to a pronounced increase in the transversal resonance peak and makes its amplitude comparable to that of the longitudinal peak.

To confirm the above qualitative explanation, we performed extensive T-matrix simulations of the extinction spectra of the overgrown NRs. Our goal was to correlate the observed experimental spectra and plasmonic shifts in Figure 4a with TEM-derived changes in NR length and width. A complete formulation of the T-matrix solvable geometrical model for NRs and other computational details can be found elsewhere.[43] Briefly, the geometrical model for each NR sample is completely determined by five parameters: the average length, the average aspect ratio and its standard deviation, and the average size and number percentage of impurity particles. The first, second, and third parameters were taken from TEM statistics (Table S1, Supporting Information, and Figure 3). In all simulations, the NRs were cylinder-shaped and had semispherical ends, the number percentage of the impurity particles was 2%, and the average size of impurities was 25% of the average NR length.

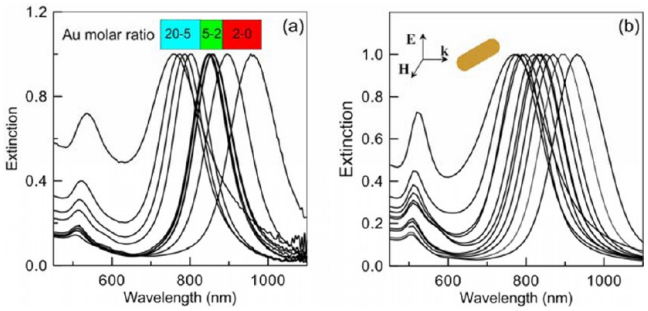

Figure 4. Experimental (a) and simulated (b) extinction spectra of the NRs obtained for overgrowth at gold molar ratios of 0 to 20. For calculations, the geometrical parameters of the NRs were taken from TEM statistical analysis.

A typical example of the calculated spectra is shown in Figure 4b. All spectra were normalized to their maxima and plotted at the same axis scale as the experimental curves in Figure 4a. In general, the simulated spectra demonstrate good agreement with experimental data both in the position of the major resonances and in changes in the relative intensities of the transversal plasmon resonances. More importantly, the simulations demonstrate a notable similarity with the experimental changes in spectral shifts during the overgrowth process. Some minor differences between simulated and observed peak positions and FWHMs of the spectra can be attributed to the model approximations, including deviations of the NR shape from exact cigars, uncertainty in the surface electron scattering constant,[53,54] and replacement of the NR statistical ensemble by a model log-normal distribution.[43]

Overgrowth Mechanism. To further evaluate the mechanism of NR overgrowth, we compared TEM images of the overgrown particles obtained with the binary surfactant mixture (0.037 M CTAB + 0.08 M NaOL) and with 0.1 M CTAB alone. The final NR morphology evolves from a subpopulation of the original NRs, presumably those with a mixture of {110}, {111}, and {110} crystal facets. The reduced overgrowth rate, together with different growth rates on these facets, mediated by the different stability of the adsorbed surfactant, leads to formation of particles with a range of shapes (Figure 5a). In the case of CTAB alone, particles with a dog-bone morphology dominated in the final product (Figure 5b). By contrast, the NaOL + CTAB overgrown NRs exhibited the cigarlike shape of their parent particles but a changed aspect ratio.

The dog-bone shape of NRs is typical of various seed-mediated CTAB-assisted synthesis protocols. According to recent reports,[55,56] dumbbell-like NRs can actually be intermediate rather than final particles because of faster growth on the tips as compared to the lateral facets. To make sure that we were dealing with the final rather than intermediate NRs, we performed additional overgrowth experiments with both CTAB and CTAB + NaOL systems. Specifically, 0.1 mL of 100 mM ascorbic acid was added to 20 mL of the overgrown samples. No changes in the optical density or in the extinction peak position were observed during the 48-h period, confirming the absence of significant quantities of unreduced gold ions. In any case, one can assume that some negligible percentage of unreduced gold ions can be presented in the growing solution only in an inactive form, i.e., as inactive complexes with surfactant that cannot contribute to the further reshaping of the NRs. The dumbbell-like shape suggests that the end {111} facet of the NRs is more amenable to overgrowth than the side

dx.doi.org/10.1021/la404399n | Langmuir 2014, 30, 1696−1703

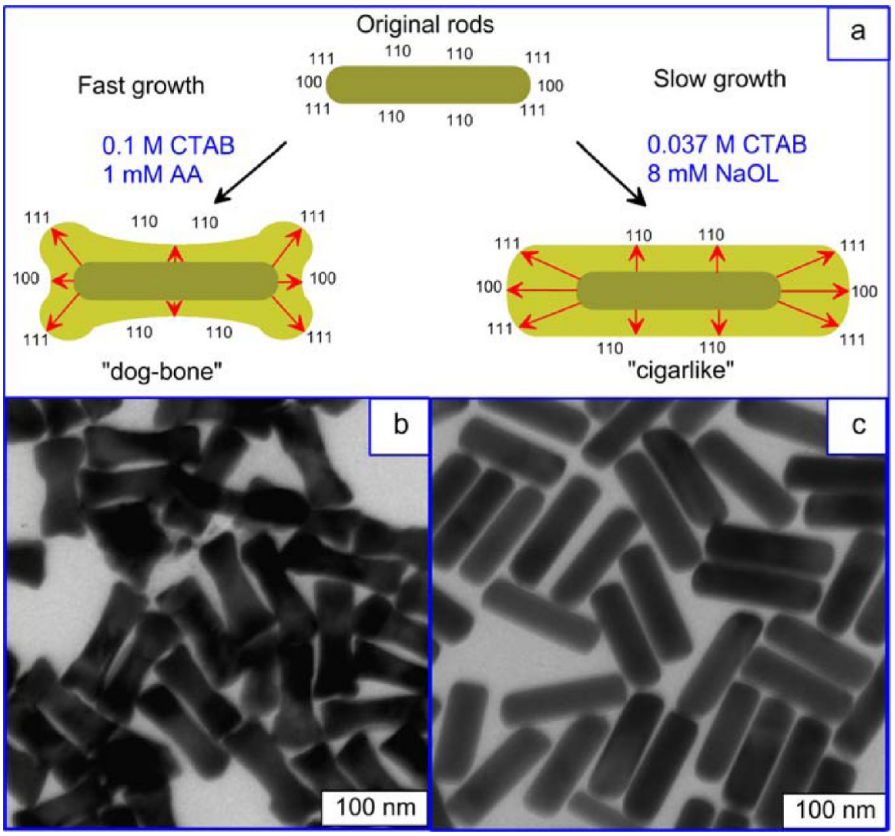

Figure 5. Schematic illustration of the fast and slow overgrowth of NRs (a). Typical TEM images obtained for NR samples after fast overgrowth by using a common 0.1 M CTAB growth solution (b) and slow overgrowth by using a binary surfactant mixture (c).

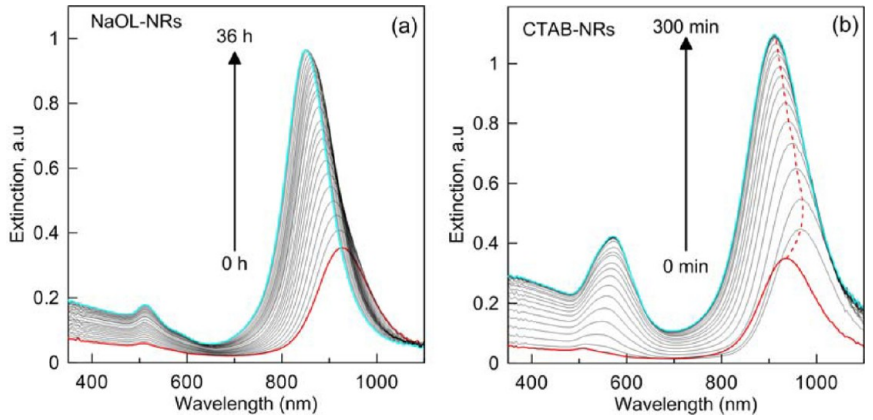

Figure 6. Evolution of the extinction spectra with time for the 0.037 M CTAB + 0.08 M NaOL (a) and 0.1 mM CTAB (b) growth solutions. The initial time steps are 1 h and 10 min for the left (a) and right (b) panels, respectively. Note the high quality ratio $A_{\parallel}/A_{\perp} = A_2/A_1$ of the plasmonic peaks, the small fwhm of the major peak, and its monotonous short-wavelength shift with time for NaOL NRs (a). By contrast, the major peak position of CTAB NRs shifts to the red first and then returns to a slightly blue-shifted position.

{110} and end {100} facets. A previous study[57] revealed that surfactants are expected to bind much more strongly to the less close packed {110} surface than to the {111} or {100} facets. Our results imply that these less stable {110} facets are unlikely to be coated with gold owing to the stronger interaction with the surfactant molecules.

Along with the interaction between surfactant molecules and gold crystalline facets, the reduced reaction rate is the key parameter which improves shape control during overgrowth in the binary NaOL + CTAB mixture. In general, NaOL can play a double role in the shape control of the overgrown NRs. On the one hand, the binary surfactant mixture improves the stability of the NR crystal facets. In this process, NaOL serves as an anionic surfactant. On the other hand, NaOL itself serves as a reductant for Au(III) ions at the first reaction stage, as the double bond in NaOL can slowly reduce Au^{3+}. Accordingly, the amount of added ascorbic acid was reduced by 8 times. The presence of NaOL in the growth solution changes the overall redox potential of the gold ions and, together with a decreased concentration of ascorbic acid, leads to a dramatic decrease in the reaction rate. Thus, the binary surfactant mixture reduces the reduction kinetics, thus inhibiting the isotropic growth. This

dx.doi.org/10.1021/la404399n | *Langmuir* 2014, 30, 1696−1703

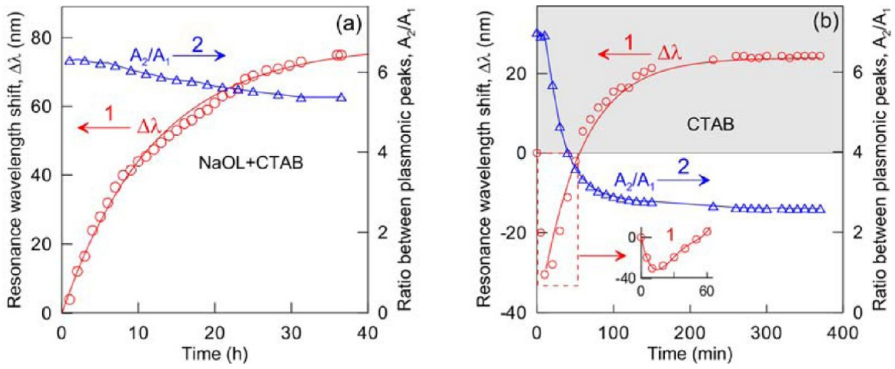

Figure 7. Time-dependent longitudinal LPR shift $\Delta\lambda(t) = \lambda(0) - \lambda(t)$ (1) and plasmonic peak ratio $A_{\parallel}/A_{\perp} = A_2/A_1$ (2) for NaOL+CTAB (a) and CTAB (b) overgrown NRs. The inset in the panel b shows an enlarged initial part of the kinetic curve $\Delta\lambda(t)$. Note the difference between the time scales in panels a and b (hours and minutes, respectively). The gray area in panel b corresponds to the actual monotonous LPR shift of CTAB NRs ($\Delta\lambda_{max} \simeq 25$ nm) from the initial LPR position. Curves 1 in panels a and b represent analytical approximations according to eqs 1 and 2, respectively.

observation is in line with the recent study by Scarabelli et al.,[56] who showed that slowing down the kinetics of reduction together with the presence of additives (such as silver ions) affects the NR morphology.

In the case of CTAB-assisted reduction, we observed fast anisotropic overgrowth, which produced dumbbell-like NRs together with irregularly shaped particles. Figure S3 in Supporting Information shows the extinction spectra of the NRs obtained by overgrowth in 0.1 CTAB at the gold molar ratio R = growth solution/seed NRs from 0 to 20. With a small increase in R from 2 to 2.5, the major peak moves to the red from 874 to 910 nm, then decreases in amplitude, and returns practically to the initial 883 nm position at R = 2.83; further, the major peak decreases and shifts to the red when the molar ratio R increases from 3.33 to 20. These spectral transformations are accompanied by strong variations in the transversal plasmonic peak.

To clarify the differences in the reduction speed for the CTAB and NaOL + CTAB systems, we performed additional kinetic experiments. To this end, the UV−vis spectra of the NR suspensions were monitored during overgrowth for both CTAB and NaOL + CTAB surfactant systems (Figure 6).

Figure 7 summarizes the evolution with time of the LPR plasmonic shift $\Delta\lambda(t) = \lambda(0) - \lambda(t)$ and the LPR peaks ratio $A_2(t)/A_1(t) = A_{\parallel}(t)/A_{\perp}(t)$ for synthesis of NRs with the CTAB and NaOL + CTAB surfactants. Curve 1 in Figure 7a represents the following analytical approximation:

$$\Delta\lambda\ (\text{nm}) = 78 \times [1 - \exp(-t/12)] \quad (1)$$

where t is expressed in hours. Similarly, the monotonous part of curve 1 in Figure 7b can be approximated by the following expression:

$$\Delta\lambda\ (\text{nm}) = 66 \times [1 - \exp(-t/55)] - 42 \quad (2)$$

where t is expressed in minutes.

The main advantage of the overgrowth protocol is the accurate control of the plasmon resonance position and geometrical parameters of the overgrown NRs. For example, the kinetic spectra in Figure 6a and the time-dependent LPR shift (1) in Figure 7a illustrate a monotonic LPR blue-shift with a 1-nm decrement every 20 min during overgrowth in the binary surfactant mixture. This means that one can tune the LPR position with an accuracy of about 1 nm by simply controlling the overgrowth time. This quality control is impossible if one varies only the reaction parameters in the original NaOL + CTAB protocol.[41] Indeed, if one compares the NR dimensions in panels a [88 × 23 nm] and d [96 × 21 nm] in Figure 1 of the paper,[41] one will note quite close geometrical parameters obtained by a small variation in the pH (1.51 to 1.36) of the growth solution. At the same time, this small variation in synthesis conditions at strongly acidic pH results in a strong 110-nm plasmonic shift from 810 to 920 nm. Our own experience shows that it is quite difficult or even impossible to reproduce NR samples with a desired location of the plasmonic peak, when NRs are fabricated at independent runs. In contrast, the overgrowth approach reduces this difficult task to simple monitoring of spectra in the reaction mixture during a slow kinetic process.

The next remarkable feature of the overgrowth protocol is the preservation of the LPR peaks ratio as illustrated by curve 2 in Figure 7a. Again, for CTAB-overgrown NRs, the quality parameter $A_2/A_1 = A_{\parallel}/A_{\perp}$ dramatically decreases from 7 to almost 2. Finally, the percentage of impurity particles also remains close to that in the seed solution of NaOL NRs. By contrast, overgrowth with CTAB results in a nonmonotonous LPR shift in the initial reaction time. Accordingly, the overall LPR tuning after the CTAB-assisted overgrowth process is only about 20 nm (Figure 7b). This should be compared to 75-nm LPR shifts for overgrowth in the NaOL + CTAB mixture (curve 1 in Figure 7a).

■ CONCLUSIONS

We have explored an easy approach to manipulating the optical behavior and geometrical properties of gold NRs by overgrowth in a binary surfactant mixture containing CTAB and NaOL. Sodium oleate serves both as a capping agent and as a reductant, leading to slow and controllable overgrowth. By contrast with overgrowth in the usual 0.1 M CTAB solution, our approach results in the formation of monodisperse cigarlike nanorods with a small amount of impurities. Both the average lengths and the average diameters of the nanoparticles grow monotonically with the progress of overgrowth, which depends on the gold molar ratio between the original NRs and the growth solution. As compared to the original NaOL + CTAB method,[41] the main advantage of the overgrowth approach is the reproducible and convenient tuning of the dimensions and plasmonic wavelength by simply controlling the reaction time and the molar ratio between seeded NRs and growth solution. In practice, we can easily achieve fine-tuning of the LPR wavelength with an accuracy of about 1 nm by a simple

dx.doi.org/10.1021/la404399n | Langmuir 2014, 30, 1696−1703

monitoring of the reaction time. In some applications, such a possibility may be very important from a practical point of view. For example, the fine-tuning of the LPR is crucial for plasmonic photothermal therapy of tumors,[58,59] trapping of particles with laser light,[60] or optoporation of cells by short laser pulses.[61]

■ ASSOCIATED CONTENT

Supporting Information

HR-TEM image of NRs obtained by overgrowth at a gold molar ratio of 2.5 (Figure S1). SEM and TEM images of the NRs after overgrowth at a very high gold molar ratio (Figure S2). A table of the geometrical and optical parameters of the NRs (Table S1). Extinction spectra of the NRs obtained by overgrowth in 0.1 M CTAB at different gold molar ratios (Figure S3). This material is available free of charge via the Internet at http://pubs.acs.org.

■ AUTHOR INFORMATION

Corresponding Author

*E-mail: bkhl@ibppm.sgu.ru.

Notes

The authors declare no competing financial interest.

■ ACKNOWLEDGMENTS

This work was supported in part by the grants from the Russian Foundation for Basic Research (12-02-00379a, 13-02-01075a, and 13-02-12413), the Government of the Russian Federation (scientific research projects implemented under the supervision of leading scientists at Russian institutions of higher education), the National Natural Science Foundation of China (No. 21375087), and the Natural Science Foundation of Shanghai (No. 13ZR1422100). V.A.K. was supported by a scholarship from the President of the Russian Federation and by a grant from OPTEC (Russia). We thank D. N. Tychinin (IBPPM RAS) for his help in preparation of the manuscript.

■ REFERENCES

(1) Chen, H.; Shao, L.; Li, Q.; Wang, J. Gold Nanorods and Their Plasmonic Properties. *Chem. Soc. Rev.* **2013**, *42*, 2679−2724.

(2) Perez-Juste, J.; Pastoriza-Santos, I.; Liz-Marzán, L. M.; Mulvaney, P. Gold Nanorods: Synthesis, Characterization and Applications. *Coord. Chem. Rev.* **2005**, *249*, 1870−1901.

(3) Khlebtsov, N. G.; Trachuk, L. A.; Melnikov, A. G. Plasmon Resonances of Silver and Gold Nanorods. *Proc. SPIE* **2004**, *5475*, 1−11.

(4) Payne, E. K.; Shuford, K. L.; Park, S.; Schatz, G. C.; Mirkin, C. A. Multipole Plasmon Resonances in Gold Nanorods. *J. Phys. Chem. B* **2006**, *110*, 2150−2154.

(5) Khlebtsov, B.; Khlebtsov, N. Multipole Plasmons in Metal Nanorods: Scaling Properties and Dependence on Particle Size, Shape, Orientation, and Dielectric Environment. *J. Phys. Chem. C* **2007**, *111*, 11516−11527.

(6) Bok, H.-M.; Shuford, K. L.; Kim, S.; Kim, S. K.; Park, S. Multiple Surface Plasmon Modes for Gold/Silver Alloy Nanorods. *Langmuir* **2009**, *25*, 5266−5270.

(7) Ye, J.; Van Dorpe, P. Improvement of Figure of Merit for Gold Nanobar Array Plasmonic Sensors. *Plasmonics* **2011**, *6*, 665−671.

(8) Lee, K.-S.; El-Sayed, M. A. Dependence of the Enhanced Optical Scattering Efficiency Relative to That of Absorption for Gold Metal Nanorods on Aspect Ratio, Size, End-Cap Shape, and Medium Refractive Index. *J. Phys. Chem. B* **2005**, *109*, 20331−20338.

(9) Ni, W.; Kou, X.; Yang, Z.; Wang, J. F. Tailoring Longitudinal Surface Plasmon Wavelengths, Scattering and Absorption Cross Sections of Gold Nanorods. *ACS Nano* **2008**, *2*, 677−686.

(10) Dykman, L.; Khlebtsov, N. Gold Nanoparticles in Biomedical Applications: Recent Advances and Perspectives. *Chem. Soc. Rev.* **2012**, *41*, 2256−2282.

(11) Durr, N. J.; Larson, T.; Smith, D. K.; Korgel, B. A.; Sokolov, K.; Ben-Yakar, A. Two-Photon Luminescence Imaging of Cancer Cells Using Molecularly Targeted Gold Nanorods. *Nano Lett.* **2007**, *7*, 941−945.

(12) Álvarez-Puebla, R. A.; Agarwal, A.; Manna, P.; Khanal, B. P.; Aldeanueva-Potel, P.; Carbó-Argibay, E.; Pazos-Pérez, N.; Vigderman, L.; Zubarev, E. R.; Kotov, N. A.; Liz-Marzán, L. M. Gold Nanorods 3D-Supercrystals as Surface Enhanced Raman Scattering Spectroscopy Substrates for the Rapid Detection of Scrambled Prions. *Proc. Natl. Acad. Sci. U.S.A.* **2011**, *108*, 8157−8161.

(13) Smith, S. L.; Gopchandran, K. G.; Ravindran, T. R.; Prasad, V. S. Gold Nanorods with Finely Tunable Longitudinal Surface Plasmon Resonance as SERS Substrates. *Nanotechnology* **2011**, *22*, 265705.

(14) Khlebtsov, B. N.; Khanadeev, V. A.; Tsvetkov, M. Yu.; Bagratashvili, V. N.; Khlebtsov, N. G. SERS Substrates Based on Self-Assembled PEGylated Gold and Gold−Silver Core−Shell Nanorods. *J. Phys. Chem. C* **2013**, *117*, 23162−23171.

(15) Dinish, U. S.; Douglas, G.; Chit Yaw, F.; Ramaswamy, B.; Winston, S.; Malini, O. Optimized Synthesis of PEG-Encapsulated Gold Nanorods for Improved Stability and Its Application in OCT Imaging with Enhanced Contrast. *Plasmonics* **2013**, *8*, 591−598.

(16) Jung, Y.; Reif, R.; Zeng, Y.; Wang, R. K. Three-Dimensional High Resolution Imaging of Gold Nanorods Uptake in Sentinel Lymph Nodes. *Nano Lett.* **2011**, *11*, 2938−2943.

(17) Lapotko, D.; Lukianova, E.; Oraevsky, A. Selective Laser Nano-Thermolysis of Human Leukemia Cells with Microbubbles Generated Around Clusters of Gold Nanoparticles. *Lasers Surg. Med.* **2006**, *38*, 631−642.

(18) Huang, X.; Jain, P. K.; El-Sayed, I. H.; El-Sayed, M. A. Plasmonic Photothermal Therapy (PPTT) Using Gold Nanoparticles. *Lasers Med. Sci.* **2008**, *23*, 217−228.

(19) Mayer, K. M.; Hafner, J. H. Localized Surface Plasmon Resonance Sensors. *Chem. Rev.* **2011**, *111*, 3828−3857.

(20) Liu, N.; Tang, M. L.; Hentschel, M.; Giessen, H.; Alivisatos, A. P. Nanoantenna-Enhanced Gas Sensing in a Single Tailored Nanofocus. *Nat. Mater.* **2011**, *10*, 631−636.

(21) Murphy, C. J.; Gole, A. M.; Hunyadi, S. E.; Stone, J. W.; Sisco, P. N.; Alkilany, A.; Kinard, B. E.; Hankins, P. Chemical Sensing and Imaging with Metallic Nanorods. *Chem. Commun.* **2008**, *7*, 544−557.

(22) Knight, M. W.; Sobhani, H.; Nordlander, P.; Halas, N. J. Photodetection with Active Optical Antennas. *Science* **2011**, *332*, 702−704.

(23) Yu, Y. Y.; Chang, S. S.; Lee, C. L.; Wang, C. R. C. Gold Nanorods: Electrochemical Synthesis and Optical Properties. *J. Phys. Chem. B* **1997**, *101*, 6661−6664.

(24) Jana, N. R.; Gearheart, L.; Murphy, C. J. Seed-Mediated Growth Approach for Shape-Controlled Synthesis of Spheroidal and Rod-like Gold Nanoparticles Using a Surfactant Template. *Adv. Mater.* **2001**, *13*, 1389−1393.

(25) Jana, N. R.; Gearheart, L.; Murphy, C. J. Wet Chemical Synthesis of High Aspect Ratio Cylindrical Gold Nanorods. *J. Phys. Chem. B* **2001**, *105*, 4065−4067.

(26) Nikoobakht, B.; El-Sayed, M. A. Preparation and Growth Mechanism of Gold Nanorods (NRs) Using Seed-Mediated Growth Method. *Chem. Mater.* **2003**, *15*, 1957−1962.

(27) Lohse, S. E.; Murphy, C. J. The Quest for Shape Control: A History of Gold Nanorod Synthesis. *Chem. Mater.* **2013**, *25*, 1250−1261.

(28) Alekseeva, A. V.; Bogatyrev, V. A.; Dykman, L. A.; Khlebtsov, B. N.; Trachuk, L. A.; Melnikov, A. G.; Khlebtsov, N. G. Preparation and Optical Scattering Characterization of Au Nanorods and their Application to a Dot-Immunogold Assay. *Appl. Opt.* **2005**, *44*, 6285−6295.

(29) Khanal, B. P.; Zubarev, E. R. Purification of High Aspect Ratio Gold Nanorods: Complete Removal of Platelets. *J. Am. Chem. Soc.* **2008**, *130*, 12634−12635.

(30) Sharma, V.; Park, K.; Srinivasaraoa, M. Shape Separation of Gold Nanorods Using Centrifugation. *Proc. Natl. Acad. Sci. U.S.A.* **2009**, *106*, 4981−4985.
(31) Akbulut, O.; MacE, C. R; Martinez, R. V.; Kumar, A. A.; Nie, Z.; Patton, M. R.; Whitesides, G. M. Separation of Nanoparticles in Aqueous Multiphase Systems through Centrifugation. *Nano Lett.* **2012**, *12*, 4060−4064.
(32) Li, S.; Chang, Z.; Liu, J.; Bai, L.; Luo, L.; Sun, X. Separation of Gold Nanorods Using Density Gradient Ultracentrifugation. *Nano Res.* **2011**, *4*, 723−728.
(33) Xiong, B.; Cheng, J.; Qiao, Y.; Zhou, R.; He, Y.; Yeung, E. S. Separation of Nanorods by Density Gradient Centrifugation. *J. Chromatogr. A* **2011**, *1218*, 3823−3829.
(34) Smith, D. K.; Korgel, B. A. The Importance of the CTAB Surfactant on the Colloidal Seed-Mediated Synthesis of Gold Nanorods. *Langmuir* **2008**, *24*, 644−649.
(35) Sohn, K.; Kim, F.; Ken, C. P.; Wu, J.; Peng, Y.; Zhou, F.; Huang, J. Construction of Evolutionary Tree for Morphological Engineering of Nanoparticles. *ACS Nano* **2009**, *3*, 2191−2198.
(36) Song, J. H.; Kim, F.; Kim, D.; Yang, P. Crystal Overgrowth on Gold Nanorods: Tuning the Shape, Facet, Aspect Ratio, and Composition of the Nanorods. *Chem.—Eur. J.* **2005**, *11*, 910−916.
(37) Kou, X.; Zhang, Sh.; Yang, Zh.; Tsung, Ch.-K.; Stuky, G. D.; Sun, L.; Wang, J.; Yan, Ch. Glutathione- and Cysteine-Induced Transverse Overgrowth on Gold Nanorods. *J. Am. Chem. Soc.* **2007**, *129*, 6402−6404.
(38) Hubert, F.; Testard, F.; Thill, A.; Kong, Q.; Tache, O.; Spalla, O. Growth and Overgrowth of Concentrated Gold Nanorods: Time Resolved SAXS and XANES. *Cryst. Growth Des.* **2012**, *12*, 1548−1555.
(39) Wang, Y.; Long, S.; Vdovic, S.; Wang, X. Fine Tuning of the Longitudinal Plasmon Resonance of Gold Nanorods by Depleting Gold Precursor. *Chem. Mater.* **2013**, *25*, 1372−1376.
(40) Ratto, F.; Matteini, P.; Rossi, F.; Pini, R. Size and Shape Control in the Overgrowth of Gold Nanorods. *J. Nanopart. Res.* **2010**, *12*, 2029−2036.
(41) Ye, X.; Zheng, Ch.; Chen, J.; Gao, Y.; Murray, C. B. Using Binary Surfactant Mixtures to Simultaneously Improve the Dimensional Tunability and Monodispersity in the Seeded Growth of Gold Nanorods. *Nano Lett.* **2013**, *13*, 765−771.
(42) Ye, X.; Gao, Y.; Chen, J.; Reifsnyder, D. C.; Zheng, C.; Murray, C. B. Seeded Growth of Monodisperse Gold Nanorods Using Bromide-Free Surfactant Mixtures. *Nano Lett.* **2013**, *13*, 2163−2171.
(43) Khlebtsov, B.; Khanadeev, V.; Pylaev, T.; Khlebtsov, N. A New T-Matrix Solvable Model for Nanorods. *J. Phys. Chem. C* **2011**, *115*, 6317−6323.
(44) Khlebtsov, B. N.; Khanadeev, V. A.; Khlebtsov, N. G. Observation of Extra-High Depolarized Light Scattering Spectra from Gold Nanorods. *J. Phys. Chem. C* **2008**, *112*, 12760−12768.
(45) Eustis, S.; El-Sayed, M. A. Determination of the Aspect Ratio Statistical Distribution of Gold Nanorods in Solution from a Theoretical Fit of the Observed Inhomogeneously Broadened Longitudinal Plasmon Resonance Absorption Spectrum. *J. Appl. Phys.* **2006**, *100*, 044324.
(46) Guerrero-Martínez, A.; Pérez-Juste, J.; Carbó-Argibay, E.; Tardajos, G.; Liz-Marzán, L. M. Gemini-Surfactant-Directed Self-Assembly of Monodisperse Gold Nanorods into Standing Superlattices. *Angew. Chem., Int. Ed.* **2009**, *48*, 9484−9488.
(47) Carbó-Argibay, E.; Rodríguez-González, B.; Gómez-Graña, S.; Guerrero-Martínez, A.; Pastoriza-Santos, I.; Pérez-Juste, J.; Liz-Marzán, L. M. The Crystalline Structure of Gold Nanorods Revisited: Evidence for Higher-Index Lateral Facets. *Angew. Chem., Int. Ed.* **2010**, *49*, 9397−9400.
(48) Katz-Boon, H.; Rossouw, C. J.; Weyland, M.; Funston, A. M.; Mulvaney, P.; Etheridge, J. Three-Dimensional Morphology and Crystallography of Gold Nanorods. *Nano Lett.* **2011**, *11*, 273−278.
(49) Becker, J.; Zins, I.; Jakab, A.; Khalavka, Y.; Schubert, O.; Sönnichsen, C. Plasmonic Focusing Reduces Ensemble Linewidth of Silver-Coated Gold Nanorods. *Nano Lett.* **2008**, *8*, 1719−1723.
(50) Hou, Sh.; Hu., X.; Wen, T.; Liu, W.; Wu, X. Core−Shell Noble Metal Nanostructures Templated by Gold Nanorods. *Adv. Mater.* **2013**, *25*, 3857−3862.
(51) Alekseeva, A. V.; Bogatyrev, V. A.; Khlebtsov, B. N.; Mel'nikov, A. G.; Dykman, L. A.; Khlebtsov, N. G. Gold Nanorods: Synthesis and Optical Properties. *Colloid J.* **2006**, *68*, 661−678.
(52) Prescott, W.; Mulvaney, P. Gold Nanorod Extinction Spectra. *J. Appl. Phys.* **2006**, *99*, 123504.
(53) Novo, C.; Gomez, D.; Perez-Juste, J.; Zhang, Z.; Petrova, H.; Reismann, M.; Mulvaney, P.; Hartland, G. V. Contributions from Radiation Damping and Surface Scattering to the Linewidth of the Longitudinal Plasmon Band of Gold Nanorods: A Single Particle Study. *Phys. Chem. Chem. Phys.* **2006**, *8*, 3540−3546.
(54) Khlebtsov, N. G.; Dykman, L. A. Optical Properties and Biomedical Applications of Plasmonic Nanoparticles. *J. Quant. Spectrosc. Radiat. Transfer* **2010**, *111*, 1−35.
(55) Park, K.; Drummy, L. F.; Wadams, R. C.; Koerner, H.; Nepal, D.; Fabris, L.; Vaia, R. A. Growth Mechanism of Gold Nanorods. *Chem. Mater.* **2013**, *25*, 555−563.
(56) Scarabelli, L.; Grzelczak, M.; Liz-Marzán, L. M. Tuning Gold Nanorod Synthesis through Pre-reduction with Salicylic Acid. *Chem. Mater.* **2013**, *25*, 4232−4238.
(57) Nikoobakht, B.; El-Sayed, M. A. Evidence for Bilayer Assembly of Cationic Surfactants on the Surface of Gold Nanorods. *Langmuir* **2001**, *17*, 6368−6374.
(58) von Maltzahn, G.; Park, J. H.; Agrawal, A.; Bandaru, N. K.; Das, S. K.; Bhatia, S. N. Computationally Guided Photothermal Tumor Therapy Using Long-Circulating Gold Nanorod Antennas. *Cancer Res.* **2009**, *69*, 3892−3900.
(59) Khlebtsov, B. N.; Panfilova, E. V.; Terentyuk, G. S.; Maksimova, I. L.; Ivanov, A. V.; Khlebtsov, N. G. Plasmonic Nanopowders for Photothermal Therapy of Tumors. *Langmuir* **2012**, *28*, 8994−9002.
(60) Selhuber-Unkel, C.; Zins, I.; Schubert, O.; Sönnichsen, C.; Oddershede, L. B. Quantitative Optical Trapping of Single Gold Nanorods. *Nano Lett.* **2008**, *8*, 2998−3003.
(61) Lalonde, B. S.-L.; Boulais, É.; Lebrun, J.-J.; Meunier, M. Visible and Near Infrared Resonance Plasmonic Enhanced Nanosecond Laser Optoporation of Cancer Cells. *Biomed. Opt. Express* **2013**, *4*, 490−499.